Available online at www.sciencedirect.com
SCIENCE DIRECT®
International Journal of Heat and Mass Transfer 48 (2005) 793–807
International Journal of HEAT and MASS TRANSFER
www.elsevier.com/locate/ijhmt

Effects of variable properties and non-uniform heating on natural convection flows in vertical channels

J. Hernández [a,*], B. Zamora [b]

[a] Dept. de Mecánica, ETSII, UNED, Ciudad Universitaria, E-28040 Madrid, Spain
[b] Dept. de Ingeniería Térmica y de Fluidos, UPCT, E-30202 Cartagena, Spain

Received 26 March 2003

Abstract

The effects of variable properties and non-uniform heating on laminar air flows induced by natural convection in vertical channels are investigated numerically. A full-elliptic model which accounts for variations in viscosity and thermal conductivity with temperature and which determines the density from the state equation has been applied to cases in which variable property effects cannot be neglected (including conditions for which flow reversals may occur). The influence of the Rayleigh number and non-uniformity of the wall heat flux distribution on the critical heat per unit time transferred from the walls in symmetric and asymmetric channels is analyzed for a wide range of Rayleigh numbers. It is shown that the maximum wall temperature can be reduced substantially by selecting an appropriate wall heat flux distribution, although at the cost of slightly more restrictive critical conditions.

Keywords: Natural convection; Variable properties; Non-uniform heating; Critical heat flux

1. Introduction

Typical applications of laminar flows induced by natural convection in vertical two-dimensional channels formed by parallel plates include, among others, the cooling of electronic and microelectronic equipment, heat exchangers and the nuclear reactor industry. To analyze these flows, the Boussinesq approximation is usually employed when the typical temperature difference in the flow is sufficiently small compared with the absolute temperature. However, in the cooling of electronic equipment, for example, it is relatively frequent to find circumstances in which variable property effects are significant and cannot be neglected. While this type of flow has been investigated extensively, the study of variable property effects has received more limited attention.

A number of authors have used the partial Boussinesq approximation (density variation in the body force term of the vertical momentum equation only) to analyze the influence of variable thermophysical properties (generally viscosity and thermal conductivity and, in some cases, specific heat) on the flow structure and overall heat transfer in vertical channel flows (e.g., [19,6,5,1]) and in steady or transient flows inside enclosures (e.g., [8,13]). Fewer studies have additionally relaxed the Boussinesq approximation (considering the effects of density variations with temperature, using a state

* Corresponding author.
E-mail address: jhernandez@ind.uned.es (J. Hernández).

0017-9310/$ - see front matter © 2004 Elsevier Ltd. All rights reserved.
doi:10.1016/j.ijheatmasstransfer.2004.09.024

Nomenclature

b	channel width
c_p	specific heat at constant pressure
C_1, C_2	constants in Eq. (10)
g	gravitational acceleration
Gr	Grashof number, $\rho_\infty^2 g H_v b^3/\mu_\infty^2$
h	length of a discrete heat source
H_v	dimensionless heating intensity, $(T_w - T_\infty)/T_\infty$; $\bar{q}b/(k_\infty T_\infty)$
L	channel height
k	thermal conductivity
K	constant in Eq. (16), C_1/T_∞
$\dot{m}$	mass flow rate
n	number of heated plates in the channel
Nu	Nusselt number
N_x, N_y	number of grid nodes
p	pressure
P	dimensionless pressure defect
Pr	Prandtl number
q	local wall heat flux
$\bar{q}$	wall heat flux averaged over the two channel plates
r	dimensionless quantity defined in Eq. (22)
Ra	Rayleigh number, $Gr\,Pr$
Ra^*	modified Rayleigh number, $Ra(b/L)$
s	parameter in Eq. (12)
T	temperature
T^*	dimensionless temperature, T/T_∞
T_L	temperature at $x = L$
T_w	wall temperature
T_∞	ambient temperature
u, v	velocity components
U, V	dimensionless velocity components
x, y	coordinates (Fig. 1)
X, Y	dimensionless coordinates
x^*	x coordinate made dimensionless with channel height
x_i	center coordinate of the discrete heat source i
x_t	thermal entrance length

Greek symbols

θ	dimensionless temperature, $(T - T_\infty)/(H_v T_\infty)$
μ	dynamic viscosity
ρ	density

Subscripts

b	Boussinesq approximation and constant properties
∞	ambient condition

Superscript

$'$	quantity made dimensionless with the ambient value

equation) to analyze flows in a vertical plate ([16], where water is the fluid considered), vertical channels (e.g., [12,22]) and within enclosures [4,20]. Different studies have been carried out to analyze the limit of application of the Boussinesq approximation [9,24,4]. This approximation can lead to significant errors in the velocity and temperature fields when temperature differences are above a value in the order of 20% of the mean temperature, although even for temperature differences in the region of 60% it can provide accurate estimations of the overall heat transfer coefficients [4].

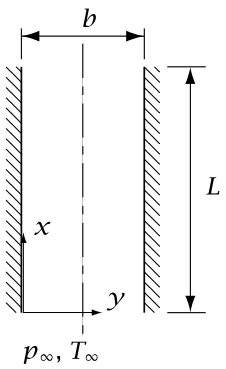

Fig. 1. Schematic representation of the channel.

Guo and Wu [12] carried out an investigation into the influence of variable property effects on the air flow induced by natural convection in vertical channels. Their numerical results for symmetrically-heated channels, which were obtained using a parabolic model, showed that both the dimensionless mass flow rate and the Nusselt number in the channel may be noticeably lower than those obtained assuming constant properties and the Boussinesq approximation. They also showed that the effect of density variation (thermal drag) is responsible for the non-monotonic dependence of the induced mass flow rate on the wall temperature or wall heat flux and that, when the wall heat flux is fixed and reaches a critical value, the wall temperature increases sharply and exhibits a crisis phenomenon similar to burnout in flow boiling.

In a previous work [22], we made a numerical analysis of how variable property effects influence the induced mass flow rate and the size of the recirculation region in

a channel formed by isothermal and adiabatic plates. We found that such effects considerably reduce the size of the recirculation region, which decreases almost linearly with the dimensionless temperature difference. The numerical results obtained for the mass flow rate induced in the channel pointed to a general trend which reflected those seen in previous works carried out for symmetric heating conditions [11,12,10]. However, for certain ranges of parameters that roughly coincide with those for which flow reversals exist, variable property effects increase the mass flow rate induced in the channel. This increase and the reduction in the size of the reverse flow region were explained by the change in the flow pattern that variable property effects produce.

The use of isothermal or isoflux boundary conditions in channels with symmetric or asymmetric heating may yield results of acceptable accuracy in the calculation of the thermal performance of many configurations of interest (see, for example, [2]). However, it is also frequent to encounter practical situations in which the effects of non-uniform heating of the channel plates must be taken into account. Furthermore, when a given global heat flux must be transferred from the plates to the fluid, and plate heating can be described by imposing boundary conditions of the Neumann type, it may be interesting to determine heat flux distributions along the wall that minimize the maximum wall temperature. This is especially so in the cooling of electronic printed circuits, for example, in which an appropriate arrangement of the dissipating components can contribute to reducing the maximum temperature reached in these components and, consequently, their risk of being damaged.

To our knowledge, all previous studies on variable property effects in vertical-channel flows have been carried out for uniform wall heating conditions. The influence of non-uniform heating conditions in channels with partially heated walls or walls with discretely heated elements, has been studied by different authors using the Boussinesq approximation and assuming constant properties. Wang et al. [21] made a numerical analysis of the cooling of discretely heated integrated circuit packages mounted on a vertical board. Lee [14] carried out a combined numerical and theoretical investigation into laminar natural convection heat and mass transfer in vertical parallel plates with unheated entry and exit. Bianco et al. [3] studied experimental and numerically natural convection flows in isoflux inclined channels, discretely heated inclined channels and uniformly heated channels with adiabatic extensions, in which they demonstrated the influence of different geometrical parameters on the Nusselt number.

In this work we investigate the influence of variable property effects on natural-convection air flows in vertical channels under non-uniform heating and non-Boussinesq conditions. More specifically, the main objectives are the following: (1) To analyze the effects of the Rayleigh number and non-uniformity of the wall heat flux on the critical value of the average wall heat flux above which the burnout phenomenon described by Guo and Wu [12] occurs. (2) To study, for a wide range of Rayleigh numbers and dimensionless average wall heat fluxes, the influence of variable property effects and non-uniformity of the wall heat flux on the wall temperature distribution (in particular, on the value and location of the maximum wall temperature). For this purpose, we use an elliptic model in which effects of density, viscosity and thermal conductivity variations are taken into account, and compare the results with those obtained using the Boussinesq approximation and assuming constant properties. The numerical results for the critical wall heat flux are also compared with estimations derived analytically in Section 3.

2. Mathematical model

The full-elliptic two-dimensional conservation equations governing the steady fluid flow in the channel, when variable property effects are taken into account, can be written in dimensionless form as follows (see, e.g., [22]):

$$\frac{\partial(\rho' U)}{\partial X}+\frac{\partial(\rho' V)}{\partial Y}=0, \tag{1}$$

$$\rho'\left(U\frac{\partial U}{\partial X}+V\frac{\partial U}{\partial Y}\right)=-\frac{\partial P}{\partial X}+\frac{1}{Gr^2}\frac{\partial}{\partial X}\left(\mu'\frac{\partial U}{\partial X}\right)+\frac{\partial}{\partial Y}\left(\mu'\frac{\partial U}{\partial Y}\right)+\frac{1-\rho'}{H_v}, \tag{2}$$

$$\rho'\left(U\frac{\partial V}{\partial X}+V\frac{\partial V}{\partial Y}\right)=-Gr^2\frac{\partial P}{\partial Y}+\frac{1}{Gr^2}\frac{\partial}{\partial X}\left(\mu'\frac{\partial V}{\partial X}\right)+\frac{\partial}{\partial Y}\left(\mu'\frac{\partial V}{\partial Y}\right), \tag{3}$$

$$\rho'\left(U\frac{\partial \theta}{\partial X}+V\frac{\partial \theta}{\partial Y}\right)=\frac{1}{Pr\,Gr^2}\frac{\partial}{\partial X}\left(k'\frac{\partial \theta}{\partial X}\right)+\frac{1}{Pr}\times\frac{\partial}{\partial Y}\left(k'\frac{\partial \theta}{\partial Y}\right), \tag{4}$$

where the following dimensionless quantities appear:

$$X=\frac{x}{b\,Gr},\quad Y=\frac{y}{b},\quad U=\frac{\rho_\infty u b}{\mu_\infty Gr},\quad V=\frac{\rho_\infty v b}{\mu_\infty}$$
$$P=\frac{(p-p_\infty)\rho_\infty b^2}{\mu_\infty^2 Gr^2},\quad \theta=\frac{T-T_\infty}{H_v T_\infty}, \tag{5}$$

$$Gr=\frac{\rho_\infty^2 g H_v b^3}{\mu_\infty^2},\quad Pr=\frac{\mu_\infty c_p}{k_\infty},\quad \rho'=\frac{\rho}{\rho_\infty},$$
$$\mu'=\frac{\mu}{\mu_\infty},\quad k'=\frac{k}{k_\infty}, \tag{6}$$

where u and v are the velocity components along the x and y coordinates (see Fig. 1); p is the pressure; p_∞ is the ambient pressure, which satisfies $dp_\infty/dx = -\rho_\infty g$; H_v is the heating intensity (following the notation used in [12]), defined below as a dimensionless characteristic temperature difference or heat flux, and L and b are the channel height and width, respectively. The specific heat is considered as constant. Since in a previous work [22] we found that recirculation effects may affect the way in which variable property effects modify the flow pattern, we have retained the terms that give a full elliptic character to the governing equations. Heat transfer by radiation has been neglected, which may only be advisable for low wall temperatures, as will be discussed later.

This work mainly focuses on heating conditions which can be represented with acceptable accuracy by fixed heat flux distributions along the walls, and which are encountered, for example, in the natural-convection cooling of rack-mounted printed circuit boards of electronic equipment. In these cases, the heating intensity is defined as

$$H_v = \frac{\bar{q} b}{k_\infty T_\infty}, \tag{7}$$

where $\bar{q}$ is the average (over the two channel plates) wall heat flux. In isothermal cases, for which we also present some results in this paper for validation purposes, the heating intensity is defined as

$$H_v = (T_w - T_\infty)/T_\infty, \tag{8}$$

where T_w is the wall temperature. In the channel configurations that will be considered here, either one or both of the channel walls are heated. In the first case, the unheated wall will be kept adiabatic, and, in the second, the channel will be heated symmetrically.

Introducing the perfect gas assumption and assuming that pressure variations are negligible in the state equation, we can write

$$\rho' = T_\infty/T = 1/(1 + H_v\theta). \tag{9}$$

The following expressions for μ' and k' [19,12] will be used:

$$\mu' = \frac{(1 + H_v\theta)^{1.5}}{1 + H_v\theta/(1 + C_1/T_\infty)},$$
$$k' = \frac{(1 + H_v\theta)^{1.5}}{1 + H_v\theta/(1 + C_2/T_\infty)}, \tag{10}$$

where C_1 and C_2 are constants (in this work, only results obtained for values of $C_1/T_\infty = 0.36$ and $C_2/T_\infty = 0.66$, corresponding to air, will be presented). It should be pointed out that the results presented in this work do not change much if the expression for μ' given in Eq. (10) is used and a constant Prandtl number equal to 0.71 is assumed.

The computational domain will be restricted to the space between plates, which requires an appropriate treatment of the boundary conditions at the inlet and outlet channel sections (as will be mentioned later, this may not be completely appropriate for very low Rayleigh numbers or in near critical conditions) [22,23]. At the inlet section, the mass flow rate is assumed to be dependent on the square root of the difference between the ambient pressure and the pressure at each inlet cell, which is equivalent to assuming that the Bernoulli equation holds at the entrance region outside the channel. It is also assumed that the incoming fluid is at ambient temperature, and that heat conduction through the inlet section can be neglected. At the outlet section, the pressure is fixed at ambient pressure, $P = 0$, and streamwise variations of the velocity components and temperature are neglected. When the flow conditions give rise to zones of inflow and outflow through the outlet section, the fluid in the inflow region ($U < 0$) is assumed to enter at $\theta = 0$. A brief discussion of these types of inlet and outlet boundary conditions is presented by Desrayaud and Fichera [7]. No-slip boundary conditions are imposed at the channel walls. At heated isothermal walls, $\theta = 1$, at walls with a fixed heat flux q, $k'\partial\theta/\partial Y = q/\bar{q}$, and at adiabatic walls, $\partial\theta/\partial Y = 0$.

The solution of the governing equations in general depends on four-dimensionless parameters (Ra^*, H_v, b/L and Pr) and on the specific temperature or heat flux distribution law along the channel walls. In this work we consider a wide range of Rayleigh numbers ($0.05 \leqslant Ra^* \leqslant 10^5$) and heating intensities ($0.005 \leqslant H_v \leqslant 32$), and fixed values of $Pr = 0.71$ and $b/L = 0.04$. The influence of the Prandtl number will be investigated in future works. As will be shown later, the channel aspect ratio b/L does not appreciably affect the flow characteristics for the boundary conditions described above.

In many electronic applications in which the wall heat flux distribution is given, the maximum wall temperature is a critical parameter, and so it is appropriate to define the Nusselt number as

$$Nu = \frac{\bar{q} b}{(T_{w,max} - T_\infty)k_\infty} = \frac{H_v T_\infty}{T_{w,max} - T_\infty} = \frac{1}{\theta_{w,max}}. \tag{11}$$

The governing equations (1)–(4) were solved numerically using the Phoenics code [18] (version 3.3) for the cases presented in Section 4. The equations were discretized on a staggered, non-uniform Cartesian grid using a finite-volume procedure with a second-order, MUSCL type differencing scheme [15] for the convective terms. We also used a lower-order hybrid scheme that required somewhat finer grids to yield results of similar accuracy. A modified version of the SIMPLE algorithm proposed by Patankar and Spalding [17] was employed to solve the coupling between continuity and momentum equations through pressure. The grid was refined at the channel entrance region and near the walls. The following

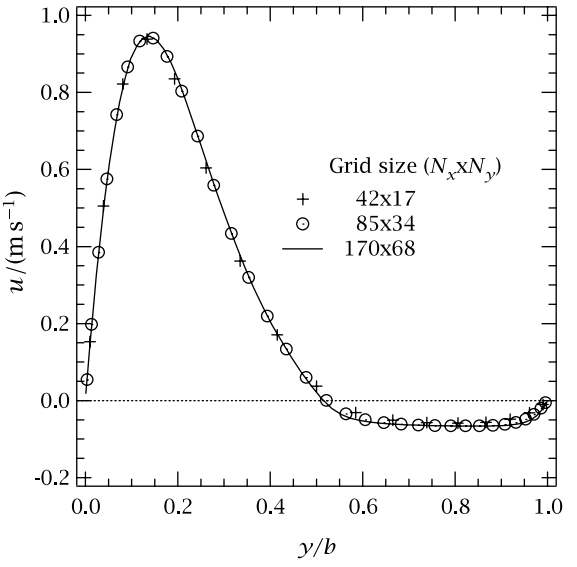

Fig. 2. Influence of the grid size on the u velocity component profile at $x = L$. Case with asymmetric heating, $q = 2\bar{q}[1 - 0.5(x/L - \frac{1}{2})]$, $Ra^* = 5 \times 10^4$, $H_v = 1$, $b/L = 0.04$ and $Pr = 0.71$.

cell size distribution was used in the y direction in each half of the channel ($j = 1$ denotes the cell at the wall): $\Delta y_j = \frac{(2j)^z - [2(j-1)]^z}{N_y^z} \frac{b}{2}$, $j = 1,\ldots,N_y/2$, with z typically varying between 1.5 and 2. A numerical solution was assumed to be converged when the L_1 norms of residuals for mass, streamwise momentum and enthalpy, divided by the flow rate of the corresponding variable through the channel inlet, became lower than 10^{-4}. A careful check for grid independence was made in order to ensure the accuracy of the computations. A grid of 85×34 ($N_x \times N_y$) cells was used to obtain all the results reported in this paper. The sensitivity of the required grid size to changes of thermal and geometric parameters was tested for a wide range of combinations. As an example, the variation of the u velocity component profile at $x = L$ with the grid size is represented in Fig. 2 for a case with asymmetric heating, a linear heat flux distribution given by $q = 2\bar{q}\left[1 - 0.5\left(x/L - \frac{1}{2}\right)\right]$, $Ra^* = 5 \times 10^4$, $H_v = 1$, $b/L = 0.04$ and $Pr = 0.71$. An increase in the grid size from 85×34 to 170×68 cells produced differences in the numerical results for the induced mass flow rate and for the maximum wall temperature of less than 0.6% and 0.3%, respectively. In general, using a grid of 85×34 cells produced nearly grid-independent results for the broad range of conditions presented in this work.

3. Analytical estimation of the critical heat flux

As mentioned above, Guo and Wu [12] described the effect of variable density on the non-monotonic variation of the induced mass flow rate with the wall temperature or wall heat flux. In isoflux channels, there is a critical value of the wall heat flux above which the wall temperature increases abruptly and a crisis phenomenon occurs. The cause for this behaviour is that, despite the increase in buoyancy that occurs with the heating intensity, the mass flow rate will decrease if the drag increases more rapidly than buoyancy, which must obviously reach a limit rather than continue to increase indefinitely.

Due to the lack of available experimental results for the critical heat flux, we were interested in comparing our numerical predictions presented in the next section with an estimation of the critical wall heat flux, which can be obtained as follows. It will be assumed that, near the critical conditions, the air temperature is uniform at any cross-section (the validity of this assumption will be discussed in Section 4). Neglecting streamwise heat conduction, the energy conservation equation reduces to $\mathrm{d}T/\mathrm{d}x = nq/(\dot{m}c_p)$ (n is the number of heated plates), which, for a channel with a non-uniform wall heat flux given by

$$q = \frac{2\bar{q}}{n}\left[1 + s\left(x^* - \frac{1}{2}\right)\right], \tag{12}$$

where $x^* = x/L$ and s is a constant, gives the following temperature distribution:

$$T^* = \frac{T}{T_\infty} = 1 + \frac{2\bar{q}L}{\dot{m}c_p T_\infty}\left[\left(1 - \frac{s}{2}\right)x^* + \frac{s}{2}x^{*2}\right]. \tag{13}$$

It will also be considered that the flow is unidirectional and that the convective term in the momentum equation, which reduces to $\rho u \partial u/\partial x = -u^2 \mathrm{d}\rho/\mathrm{d}x$, is negligible. With the above assumptions (whose validity will be discussed below), and taking into account Eqs. (9) and (10), the drag force per unit volume in the channel can be expressed as

$$F_\mathrm{d} = \int_0^L \frac{12\mu\dot{m}}{\rho b^3}\mathrm{d}x^* = \frac{12\mu_\infty \dot{m}}{b^3\rho_\infty}\left(1 + \frac{C_1}{T_\infty}\right)\int_0^L \frac{T^{*5/2}}{T^* + C_1/T_\infty}\mathrm{d}x^*, \tag{14}$$

and the buoyancy force as

$$F_\mathrm{b} = g\int_0^L (\rho_\infty - \rho)\mathrm{d}x^* = g\rho_\infty \int_0^L (1 - 1/T^*)\mathrm{d}x^*. \tag{15}$$

Equating the last member of Eqs. (14) and (15), making $C_1/T_\infty = K$ and rearranging gives

$$24\frac{H_v^2}{Ra^*}\frac{1+K}{T_L^* - 1}\int_0^L \frac{T^{*5/2}}{T^* + K}\mathrm{d}x^* = \int_0^L \left(1 - \frac{1}{T^*}\right)\mathrm{d}x^*, \tag{16}$$

where

$$T_L^* = T^*(x = L) = 1 + \frac{2\bar{q}L}{\dot{m}c_p T_\infty}. \tag{17}$$

Substituting Eq. (13) into Eq. (16) and integrating yields

$$\frac{H_v^2}{Ra^*} = \frac{\bar{q}Lv_\infty}{g\rho_\infty c_p T_\infty b^3} = \frac{(T_L^*-1)[1-I_1(T_L^*,s)]}{24(K+1)I_2(T_L^*,s)}, \tag{18}$$

where

$$I_1(T_L^*,s) = \begin{cases} \frac{1}{(T_L^*-1)r^{1/2}} \ln\left[\frac{1-(s/2-r^{1/2})^2}{1+(s/2+r^{1/2})^2}\right] \\ \quad \text{if } r>0, \\ \frac{2}{(T_L^*-1)(-r)^{1/2}}\left[\arctan\frac{1+s/2}{(-r)^{1/2}} - \arctan\frac{1-s/2}{(-r)^{1/2}}\right] \\ \quad \text{if } r<0, \end{cases} \tag{19}$$

$$\begin{aligned} I_2(T_L^*,s) = \Bigg[&(T_L^*-1)\frac{-24+44s+22s^2-3s^3}{128s^2} \\ &+\frac{1+s/2}{2s}(5/4-K)\Bigg]T_L^{*1/2} + \frac{3(1-s/2)^3}{16s^2} \\ &\times(T_L^*-1) - \frac{1-s/2}{2s}(5/4-K) \\ &+\frac{3}{8}\Bigg\{1+\frac{4}{3}K(2K-1)+(T_L^*-1) \\ &\times\frac{(1-s/2)^2}{s}\left[(T_L^*-1)\frac{(1-s/2)^2}{4s}+\frac{2}{3}K-1\right]\Bigg\} \\ &\times I_3(T_L^*,s), \end{aligned} \tag{20}$$

$$I_3(T_L^*,s) = \begin{cases} \frac{1}{[-(T_L^*-1)s/2]^{1/2}}\left[\arcsin\frac{-(1+s/2)}{r^{1/2}} - \arcsin\frac{-(1-s/2)}{r^{1/2}}\right] \\ \quad \text{if } s<0, \\ \frac{1}{[(T_L^*-1)s/2]^{1/2}}\left[\arg\cosh\frac{1+s/2}{r^{1/2}} - \arg\cosh\frac{1-s/2}{r^{1/2}}\right] \\ \quad \text{if } s>0 \text{ and } r>0, \\ \frac{1}{[(T_L^*-1)s/2]^{1/2}}\left[\arg\sinh\frac{1+s/2}{(-r)^{1/2}} - \arg\sinh\frac{1-s/2}{(-r)^{1/2}}\right] \\ \quad \text{if } s>0 \text{ and } r<0. \end{cases} \tag{21}$$

In the equations above,

$$r = (1-s/2)^2 - \frac{2s}{T_L^*-1}. \tag{22}$$

In Eq. (20) we have neglected the following term: $-K^3\int_0^L (T^*+K)^{-1}T^{*-1/2}\,dx^*$, which introduces an error of lower than 0.2% in Eq. (18) for $K = 0.36$ and the ranges of parameters considered.

Eq. (18) gives a maximum of $H_v^2/Ra^* = [H_v^2/Ra^*]_{\text{crit}}$, which can accurately be represented (with a maximum error of about 0.1% in the range $-2 \leqslant s \leqslant 2$ and a coefficient of determination $R^2 = 0.99997$) as a function of s by the following correlation:

$$\begin{aligned} [H_v^2/Ra^*]_{\text{crit}} = &-1.423\times10^{-5}s^5 - 3.474\times10^{-5}s^4 \\ &-1.777\times10^{-5}s^3 + 9.342\times10^{-5}s^2 \\ &+1.774\times10^{-3}s + 1.569\times10^{-2}, \end{aligned} \tag{23}$$

which will be compared in Fig. 14 with the numerical results presented in Section 4. For given channel geometry and ambient conditions, values of the wall heat flux above that corresponding to this maximum would produce an infinite increase of the temperature in the channel. Note that the critical heat flux increases with s, with a slope that tends to zero as s approaches a value close to 1.9, where there is a maximum. In the range $-1 \leqslant s \leqslant 1$, the linear correlation given by the last two terms of Eq. (23) reproduces the maximum of Eq. (18) with an error of lower than 0.7%.

4. Discussion of results

As already mentioned, this work mainly focuses on asymmetrically-heated channels, in which the heat flux transferred from the walls to the air is non-uniform and can be considered a given fixed value. However, we will firstly present some results for both isothermal and isoflux, symmetrically-heated channels, which will be compared with numerical and experimental results of other authors.

Predictions for the thermal entrance length in the symmetric, isothermal channel obtained in this work are compared in Fig. 3 with the corresponding numerical results of Guo and Wu [12] and with measurements obtained by means of laser speckle photography [11,10]. In the experiments, the channel length and width were $L = 100$ mm and $b = 3$ mm, and the ambient temperature was $T_\infty = 293$ K. Following Guo and Wu [12], the ther-

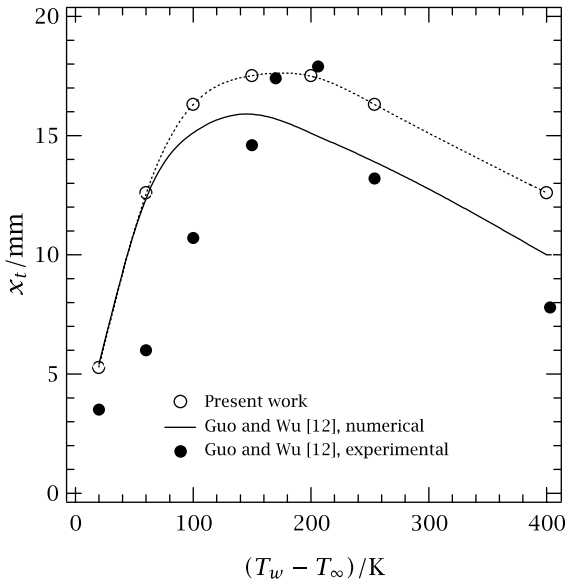

Fig. 3. Variation of the thermal entrance length with the temperature difference $T_w - T_\infty$ in a symmetric, isothermal channel with $L = 100$ mm, $b = 3$ mm and $T_\infty = 293$ K.

mal entrance length was taken as the distance from the channel entrance section to the location where the transverse density gradient at the plate surface became $2\times10^{-3}\,\mathrm{kg\,m^{-3}\,mm^{-1}}$. Note that the agreement between the two sets of numerical results is good for low temperature differences but deteriorates as variable property effects increase. The results of the present work better reproduce the maximum of x_t measured in the experiments, but yield greater discrepancies for higher temperature differences. The reasons for the differences between the numerical results of the present work and those of Guo and Wu [12] are not clear, but cannot solely be attributed to the different character of the partial differential equations solved in their respective elliptic and parabolic models. We also found that possible differences in the laws used to describe the dependence of the thermophysical properties on temperature do not change the results substantially.

Fig. 4 shows a comparison between the experimental and numerical results for the temperature distribution in a cross-section of an isothermal channel, in which the edge effects are expected to be negligible [11,10]. The agreement between the numerical results of Guo et al. [11,10] and ours is again very good when properties are assumed to be constant, whereas for variable properties the numerical results of the above authors are in good agreement with the experimental measurements while the present model gives slightly higher temperatures.

The results obtained in this work for the mass flow rate induced in isoflux channels with $b/L = 0.03$ and

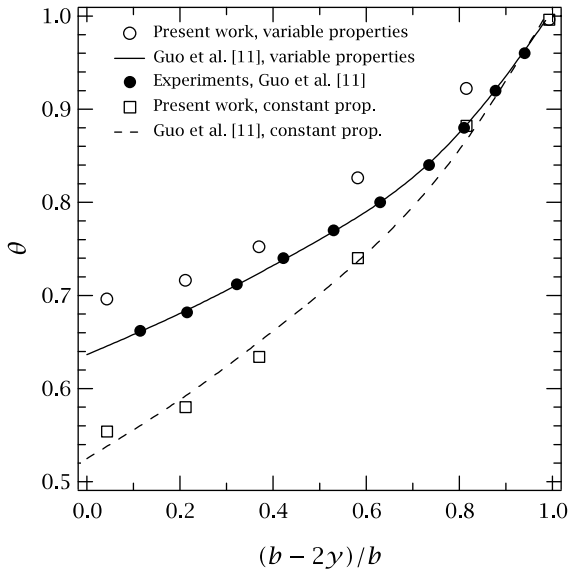

Fig. 4. Temperature profile in a cross-section at $x = 25\,\mathrm{mm}$, in a symmetric, isothermal channel with $T_w - T_\infty = 50\,\mathrm{K}$, $Pr/Ra^* = 0.44$, $b = 5\,\mathrm{mm}$ and $T_\infty = 293\,\mathrm{K}$.

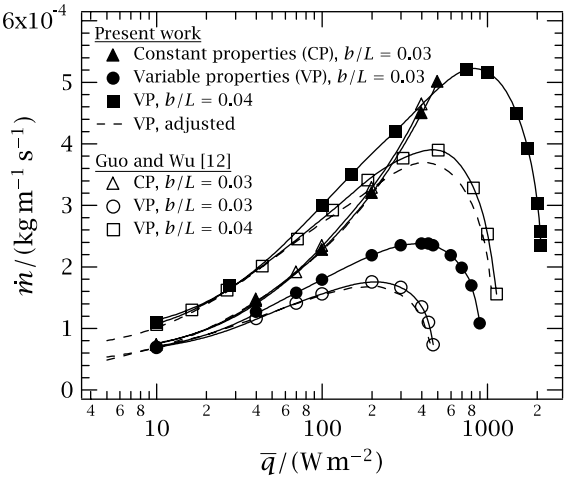

Fig. 5. Mass flow rate induced in a symmetric, isoflux channel as a function of the wall heat flux. $b/L = 0.03$, $L = 10\,\mathrm{cm}$, $T_\infty = 300\,\mathrm{K}$.

0.04, $L = 10\,\mathrm{cm}$ and $T_\infty = 300\,\mathrm{K}$ are compared in Fig. 5 with the corresponding numerical results obtained by Guo and Wu [12] using a parabolic model. It can be observed that the agreement is again very good when properties are assumed to be constant. However, when variable property effects are taken into account, and despite the overall qualitative good agreement, our results predict a value of the critical heat flux which is almost exactly twice the value obtained by Guo and Wu [12]. In fact, a very good agreement is found if the results for $\dot{m}$ obtained in the present work and the corresponding values of Ra^* are divided by $\sqrt{2}$ and 2, respectively. The results modified in this way, which are also represented in Fig. 5 with dashed lines, agree very well with those of Guo and Wu [12], which suggests that some inconsistency may exist between the values of the parameters used in [12] and in this work to define the problem conditions, as discussed below. It should be pointed out that although this inconsistency would also apply to the constant property results, the dependence of $\dot{m}$ on the square root of $\bar{q}$ in this case means that the rescaling of the results has no apparent effect because the corresponding curves become superposed.

4.1. Critical wall heat flux in isoflux and isoflux/adiabatic channels

4.1.1. Symmetric isoflux channel

The values of the critical heat flux obtained numerically for a symmetric, isoflux channel with an aspect ratio of 0.04 and different values of Ra^* can be deduced from Fig. 6. The ratio $\dot{m}/\dot{m}_b$ between the numerical results for the mass flow rate obtained taking into account variable property effects and that calculated using the

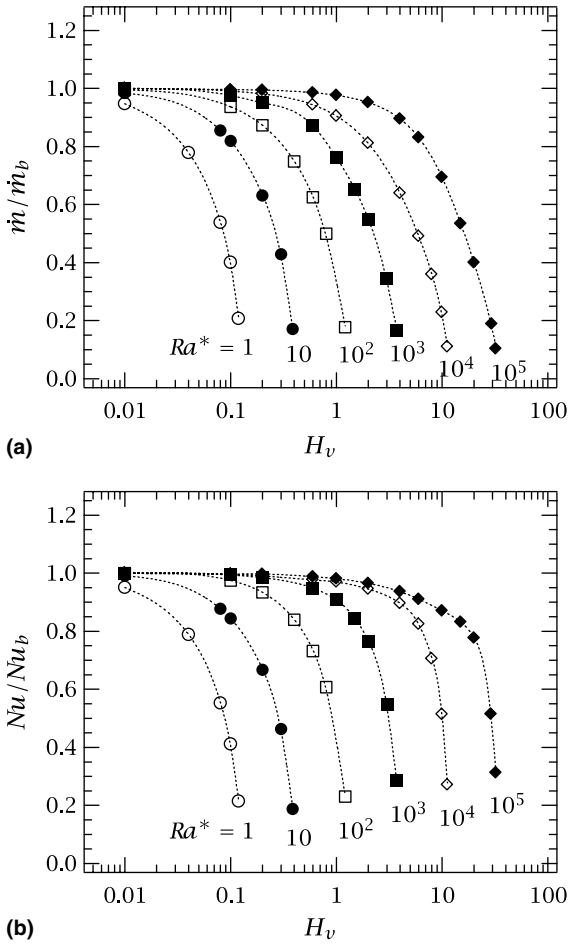

Fig. 6. Ratios $\dot{m}/\dot{m}_b$ and Nu/Nu_b as a function of the heating intensity, for symmetric, isoflux channels with $b/L = 0.04$.

Boussinesq approximation and assuming constant properties, is represented in Fig. 6(a) as a function of H_v. Fig. 6(b) shows the corresponding results for Nu/Nu_b. Notice that $\dot{m}/\dot{m}_b \simeq Nu/Nu_b$ when Ra^* is sufficiently small. For each curve, the point corresponding to the highest value of H_v is the last one for which a numerical solution could be found (except for $Ra^* = 10^6$ and 10^7, for which the critical condition is reached at higher values of H_v). For a value of H_v between 0.01% and 0.1% higher than this heating intensity (which will be taken as the critical heating intensity), the wall temperature increases dramatically and the numerical procedure diverges.

The critical values of the ratio H_v^2/Ra^* for the cases of Fig. 6 are represented with open circles in Fig. 7 as a function of the modified Rayleigh number. Given the broad ranges of parameters considered ($0.05 \leqslant Ra^* \leqslant 10^5$ and $0.02 \leqslant H_v \leqslant 32$), these critical values are in acceptable qualitative agreement with the correlation between the dimensionless critical heat flux and the

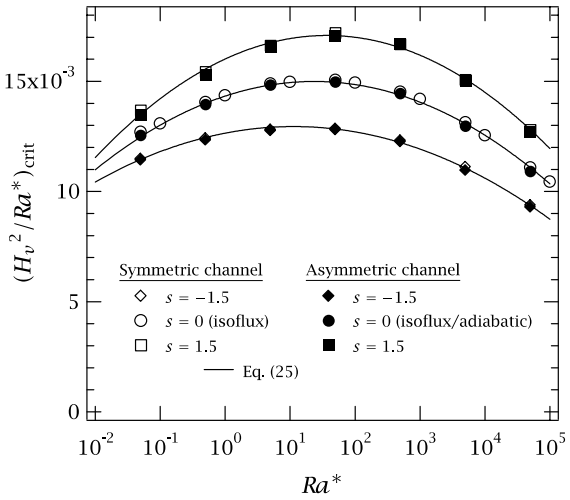

Fig. 7. Numerical results for the critical ratio H_v^2/Ra^* as a function of Ra^* for different heating conditions. Comparison with the correlation given by Eq. (25).

modified Rayleigh number proposed by Guo and Wu [12]:

$$(H_v^2/Ra^*)_{crit} = C, \tag{24}$$

where C is a constant. However, Guo and Wu [12], after fitting Eq. (24) to their numerical results, proposed a value of $C = 7.5 \times 10^{-3}$ (for H_v and Ra^* based on b), whereas we found a maximum value of $(H_v^2/Ra^*)_{crit} = 15 \times 10^{-3}$ for Ra^* around 25, which is very close to the maximum of Eq. (18) for $s = 0$. The factor of 2 between this maximum and the value of C proposed by Guo and Wu reflects the already mentioned discrepancy between our results and those of these authors in Fig. 5. This factor would be justified if the magnitude $\bar{q}$ used by Guo and Wu [12] were defined as the total wall heat flux (including both plates), although it is difficult to deduce this from their paper. For values of Ra^* far from the maximum, $(H_v^2/Ra^*)_{crit}$ tends to decrease appreciably and is about 15% and 30% lower than this maximum for $Ra^* = 5 \times 10^{-2}$ and 10^5, respectively.

The influence of the channel aspect ratio on $(H_v^2/Ra^*)_{crit}$ has been found to be negligible for the ranges of parameters considered. Only for small values of the Rayleigh number and large aspect ratios (b/L) are effects of heat conduction through the channel inlet and outlet sections, which we have neglected, expected to produce a dependence of $(H_v^2/Ra^*)_{crit}$ on b/L and make the critical values of the wall heat flux higher than those obtained numerically in this work. This dependence could be investigated by modifying the inlet and outlet boundary conditions used in the present work and introducing upstream and downstream extensions of the computational domain. However, the characteristics of these domain extensions and the conditions to be

imposed on its boundaries would depend on the particular configuration of the entrance and exit regions of the channel [23], and therefore a general solution could not be obtained. In any case, the results obtained in this work for the critical wall heat flux at low Rayleigh numbers can be considered as a lower limit for the thermal design of this type of cooling system.

Radiation effects cannot be neglected when the wall temperature becomes too high, and are more relevant for high values of Ra^* and large channel aspect ratios. However, radiation effects are not expected to change the essential characteristics of the critical phenomenon, as discussed in [12], although they will tend to increase the critical wall heat flux. This again makes the numerical results for $(H_v^2/Ra^*)_{\text{crit}}$ obtained in this work a lower limit, which can be used as a conservative criterion for the thermal analysis and design when radiation effects are relevant.

4.1.2. Asymmetric isoflux/adiabatic channel

Fig. 8 shows the same type of results of Fig. 6 for a channel with $b/L = 0.04$ and asymmetric isoflux heating conditions (adiabatic/isoflux walls). As in the case of isothermal channels [22], and despite the fact that a recirculation zone adjacent to the adiabatic wall appears at the end of the channel in some cases, the influence of the channel aspect ratio on $\dot{m}/\dot{m}_b$ has been found to be negligible for the range considered ($0.02 \leqslant b/L \leqslant 0.08$). As an example, the results for $b/L = 0.08$ and $Ra^* = 5 \times 10^4$ have also been represented in Fig. 8, where no differences from the results for $b/L = 0.04$ are noticeable.

As in the case of isothermal channels [22], for sufficiently large values of Ra^* and within a certain range of H_v, $\dot{m}$ is higher than $\dot{m}_b$. The physical reason for this behaviour, explained by Zamora and Hernández [22] for isothermal channels, is that, for such ranges of parameters, variable property effects produce a decrease, rather than an increase, of the viscous drag that compensates the corresponding reduction in buoyancy. This reduction in viscous drag is due to the modification that variable property effects produce in the flow pattern, in which the temperature and velocity profiles extend farther into the channel from the hot wall. The consequent reduction in the velocity gradients at the hot wall produces an appreciable decrease of the viscous drag for the conditions corresponding to cases with $\dot{m}/\dot{m}_b > 1$ in Fig. 8(a). As an example, Fig. 9 shows a comparison of velocity vector distributions corresponding to a case with $Ra^* = 5 \times 10^4$ and $H_v = 6$, with and without variable property effects taken into account. In some cases, the drag reduction at the hot wall may be compensated by an increase of friction at the adiabatic wall. The increase in $\dot{m}$ produced by variable property effects described above has only been found for asymmetric heating conditions for which flow reversals occur, so

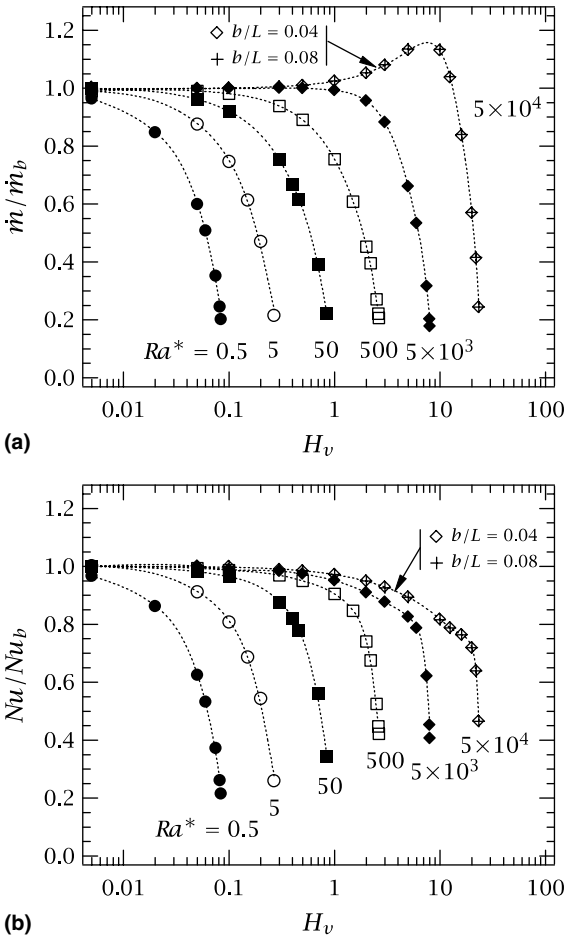

Fig. 8. Ratios $\dot{m}/\dot{m}_b$ and Nu/Nu_b as a function of the heating intensity, for asymmetric, isoflux channels with $b/L = 0.04$.

that an elliptic model is required to reproduce such effect.

As for symmetric heating conditions, the influence of the channel aspect ratio on $(H_v^2/Ra^*)_{\text{crit}}$ has also been found to be negligible, and comments similar to those made in the previous section apply.

It can be observed from Fig. 7 that there are very slight differences between the numerical results for the critical value $(H_v^2/Ra^*)_{\text{crit}}$ for symmetric and asymmetric heating (notice that $\bar{q}$ in Eq. (7) is defined as the wall heat flux averaged over the whole plate surface area, including the adiabatic wall in the asymmetric case).

4.1.3. Channels with non-uniform wall heat flux

We have already mentioned that it may be of interest in practical situations to investigate the possibility of reducing the maximum wall temperature in a channel by using an appropriate spatial distribution of the total heat per unit time to be transferred from the plates. In

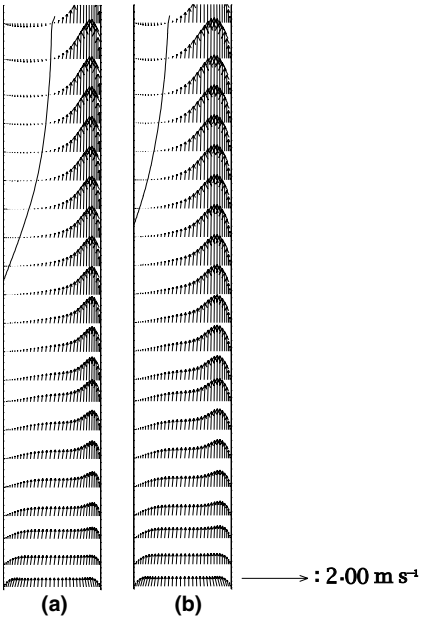

Fig. 9. Numerical results for the velocity vector distribution corresponding to a case with asymmetric heating, $Ra^* = 5 \times 10^4$ and $H_v = 3$. (a) Boussinesq model; and (b) taking into account variable property effects.

this respect, it is also interesting to analyze the possible influence of the wall heat flux distribution law on the critical heat flux. In this section, we present numerical results for the critical wall heat flux and wall temperature distribution in both symmetric and asymmetric channels with the non-uniform wall heat flux distribution given by Eq. (12).

Fig. 7 shows results for the critical parameter $(H_v^2/Ra^*)_{\text{crit}}$ as a function of Ra^*, for different values of the parameter s in the wall heat flux distribution given by Eq. (12). For any value of s, the qualitative dependence of $(H_v^2/Ra^*)_{\text{crit}}$ on Ra^* is similar to that discussed in previous sections for uniform heating conditions. Although $(H_v^2/Ra^*)_{\text{crit}}$ is relatively constant with Ra^* for intermediate values of Ra^*, which qualitatively agrees with Eq. (24) and the results of Section 3, it tends to be considerably lower for low and high Ra^* values, for which the assumptions introduced in Section 3 are less justified. The reason for the discrepancies for large values of Ra^* is that the flow is not fully developed near the critical conditions. This can be observed from Figs. 10–12, which show distributions of the dimensionless temperature obtained numerically in an asymmetrically heated channel for different Ra^* and H_v values (the highest value of H_v for which temperature contours are represented is the critical one), and wall heat flux distributions with $s = -1.5$, 0 and 1.5, respectively. Note that, for a given Rayleigh number, the temperature contours tend to become flatter as H_v increases, but the assumption of uniform temperature in any cross-section in critical conditions tend to break down as Ra^* increases. On the other hand, the effects of streamwise heat conduction are not negligible for low values of Ra^*, and tend to modify the distribution law given by Eq. (13) for critical conditions. This can be observed, for example, from Fig. 11(a), which corresponds to $Ra^* = 0.5$ and a uniform wall heat flux, for which Eq. (13) predicts temperature contours evenly spaced along the channel height, whereas Fig. 11(a) shows that, for $H_v = 0.0835$ (which is the critical value obtained numerically), the temperature tends to be uniform at the upper part of channel. The same occurs in cases with non-uniform heating, as can be seen from Figs. 10(a) and 12(a), more clearly from the second one.

It can also be observed from Fig. 7 that $(H_v^2/Ra^*)_{\text{crit}}$ increases with increasing values of s. This occurs in the

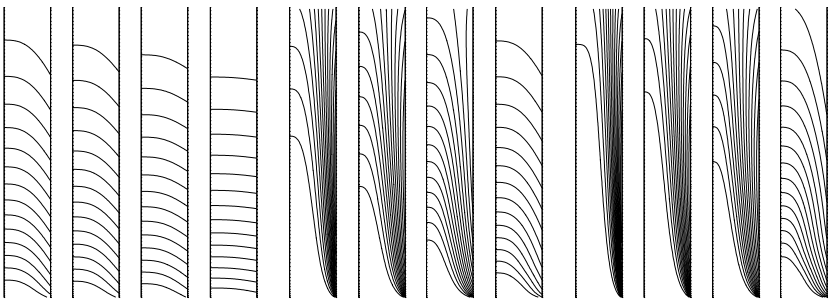

Fig. 10. Dimensionless temperature contours for three different Rayleigh numbers and different heating intensities. Case with asymmetric heating and $s = -1.5$.

range $-2 \leqslant s \leqslant 2$, except for s values very close to 2, and is explained by the fact that, for a given average heating intensity H_v, the lower s, the higher the average temperature in the channel, and so the larger the influence of variable property effects. This can be observed from Figs. 10–12. Note that, for given Ra^* and s values, the maximum temperature does not vary very much with s, whereas the region of higher temperatures at the upper part of the channel is larger for lower s values, as is to be expected.

In the ranges $-2 \leqslant s \leqslant 1.5$ and $0.05 \leqslant Ra^* \leqslant 10^5$, the numerical results for $(H_v^2/Ra^*)_{\text{crit}}$ fit very accurately (with a maximum error lower than 2% and $R^2 = 0.9972$) the following correlation:

$$(H_v^2/Ra^*)_{\text{crit}} = -(6.650 \times 10^{-5} + 1.047 \times 10^{-5} s)\ln^2(Ra^*) + (4.206 \times 10^{-4} + 1.138 \times 10^{-4} s)\ln(Ra^*) + 0.01433 + 1.123 \times 10^{-3} s. \quad (25)$$

In the whole range $-2 \leqslant s \leqslant 2.5$, the numerical results for symmetric heating fit (with a maximum error lower that 1% and $R^2 = 0.9995$) a Chebyshev bivariate polynomial in $\ln(Ra^*)$ and s of order 5, whose contours are represented in Fig. 13 (the maximum $(H_v^2/Ra^*)_{\text{crit}}$ value is reached for $s = 1.84$ and $Ra^* = 74.3$). In Fig. 14, the maximum values of H_v^2/Ra^* predicted by this polynomial for different values of s are compared with the values of $(H_v^2/Ra^*)_{\text{crit}}$ deduced analytically in Section 3, given by Eq. (23). Fig. 13 shows that these maxima are

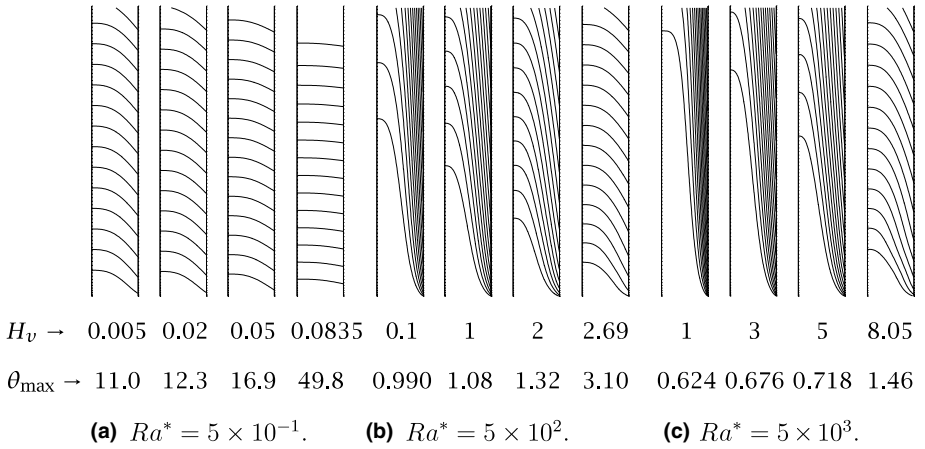

Fig. 11. Dimensionless temperature contours for three different Rayleigh numbers and different heating intensities. Case with asymmetric heating and $s = 0$.

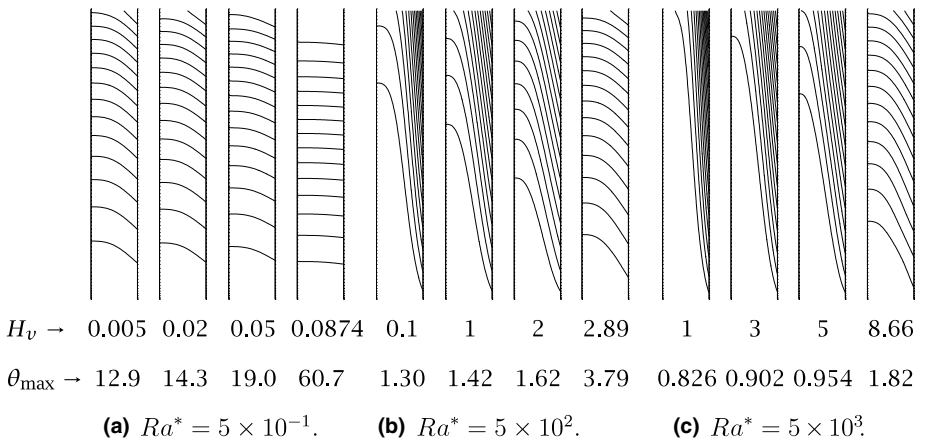

Fig. 12. Dimensionless temperature contours for three different Rayleigh numbers and different heating intensities. Case with asymmetric heating and $s = 1.5$.

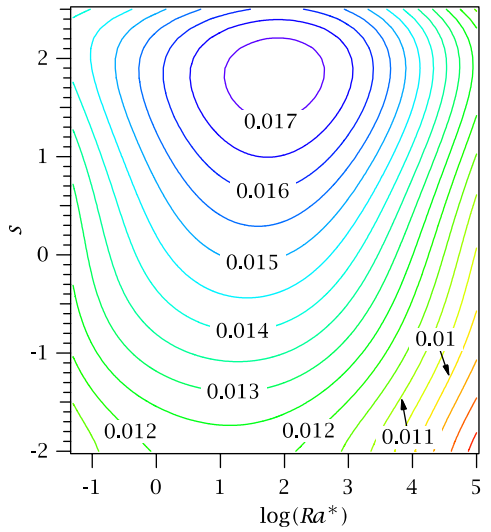

Fig. 13. Contours of the critical parameter $(H_v^2/Ra^*)_{crit}$, as given by a Chebyshev polynomial of order 5 constructed from the numerical results.

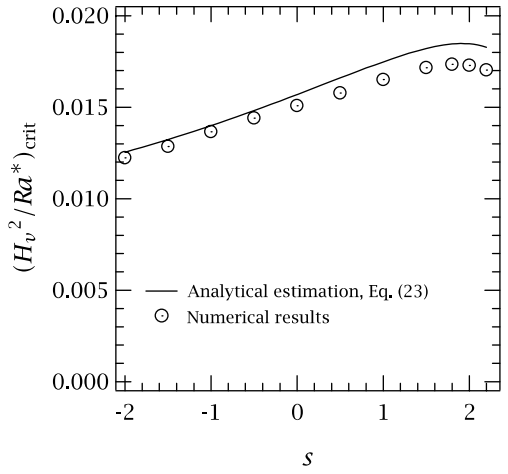

Fig. 14. Comparison between analytical estimations and numerical results for the maximum value of $(H_v^2/Ra^*)_{crit}$ as a function of parameter s.

reached at Ra^* values which increase slightly with s, varying from $Ra^* \approx 12$ for $s = -2$ to $Ra^* \approx 77$ for $s = 2$. It can be observed from Fig. 14 that there is an overall good agreement between analytical and numerical results. It is also interesting to note that the maximum of $(H_v^2/Ra^*)_{crit}$ predicted analytically near $s = 2$ is qualitatively well reproduced by the numerical model.

It should be pointed out that three-dimensional, thermal radiation and streamwise heat conduction effects will make the values of the critical heat flux higher than those predicted, for example, by Eq. (25). As already mentioned, both three-dimensional and thermal radiation effects have been neglected in the numerical model and in the analytical estimation, whereas streamwise heat conduction effects have been neglected entirely to obtain Eq. (18), and only the heat conduction through the inlet and outlet channel sections in the numerical model. If heat conduction through these sections were taken into account, its effect would depend on the channel aspect ratio and the particular configuration of the channel entrance and exit zones. This would increase the number of parameters that should be taken into account. On the other hand, the conditions for which these effects are relevant have less practical interest. As regards thermal radiation, it is expected that, as discussed in [12], its presence will not change the non-monotonic variation of mass flow rate and the critical phenomenon, except that the wall temperature will not increase indefinitely as critical conditions are approached.

4.2. Wall temperature distribution

In Fig. 15 we have represented the dimensionless temperature along a wall heated with the linear heat flux distribution given by Eq. (12), for different values of the parameter s, $H_v = 1$ and $Ra^* = 5 \times 10^4$, in a channel in which the other wall is adiabatic. It can be observed that the maximum wall temperature does not vary monotonically with s, and reaches a minimum for a value of s close to -0.5. For this optimum value of s, the maximum wall temperature is located approximately at

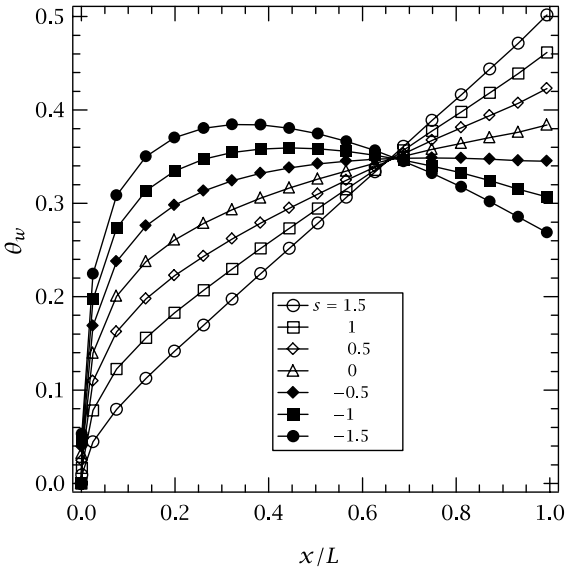

Fig. 15. Dimensionless temperature along a wall heated with the linear heat flux distribution given by Eq. (12), for different values of s, in a channel in which the other wall is adiabatic. $b/L = 0.04$, $H_v = 1$ and $Ra^* = 5 \times 10^4$.

$x/L = 2/3$. For values of s higher than this optimum, the maximum wall temperature is reached at the exit section of the channel, whereas for lower s values the maximum wall temperature is reached at $x/L < 2/3$.

When variable property effects are not relevant, the influence of s on the wall temperature distribution for other values of Ra^* and H_v is qualitatively similar to that observed from Fig. 15. However, when these effects become more relevant, they may affect not only the values of the wall temperatures, but also the optimum value of s which minimizes the maximum wall temperature and the location at which this maximum temperature is reached. This can be observed, for example, from Fig. 16, in which the dimensionless wall temperature is represented for different Ra^* and H_v values. The numerical results obtained assuming constant properties and the Boussinesq approximation are also represented. Note that for sufficiently large Ra^* or low H_v values (all cases represented except that corresponding to $H_v = 2$ and $Ra^* = 5 \times 10^2$), the temperature distributions for the three different s values considered intersect at $x/L \approx 2/3$ and the optimum value of s is clearly higher than -1, whereas for $H_v = 2$ and $Ra^* = 5 \times 10^2$ the maximum wall temperature is still reached at the channel exit section for $s = -1$, and so the optimum value of s must be lower than -1. Also note that the temperature distributions for the three different s values intersect at $x/L > 2/3$. It is also worth noting that variable property effects may produce a substantial increase of the maximum wall temperature, well above the value predicted by the non-Boussinesq model, particularly for low Ra^* and large H_v values.

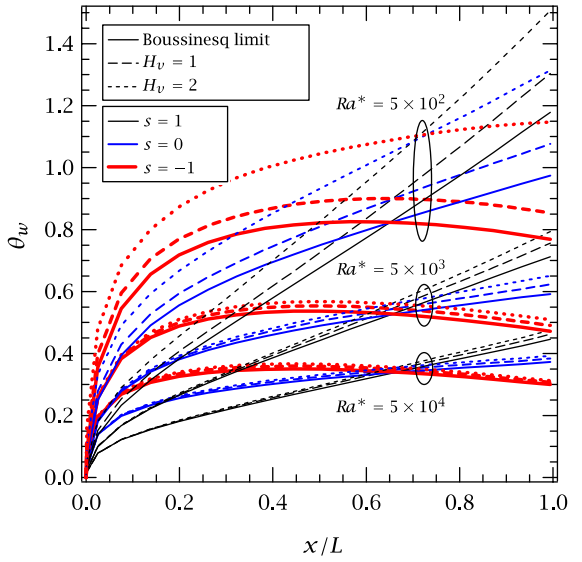

Fig. 16. Influence of the heating intensity, H_v, on the dimensionless temperature along a wall heated with the linear heat flux distribution given by Eq. (12), for different values of s and three Ra^* values, in a channel in which the other wall is adiabatic and $b/L = 0.04$.

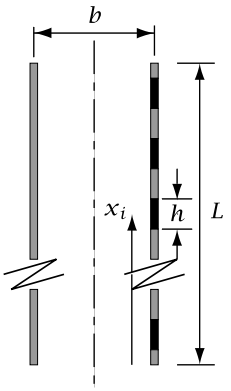

Fig. 17. Asymmetrically heated channel with N discrete, equally spaced heat sources of length h.

A heat flux distribution given by a series of discrete heat sources, such as that shown in Fig. 17, may be more realistic than a continuous one. The configuration of Fig. 17 consists of N isoflux discrete heat sources in a channel in which the unheated wall is adiabatic. The sources are equally-spaced and have strengths given by $q_i = (2\bar{q}/N)\left[1 + s\left(x_i^* - \frac{1}{2}\right)\right]$ $(i = 1, \ldots, N)$. Fig. 18 shows the dimensionless temperature along the heated wall for two values of the source length and of Ra^*. It can be observed that the maximum wall temperature follows the same general trends as in the case of the continuous heat flux distribution, and reaches a minimum for a value of s around -0.5. This minimum moves towards more negative values of the slope s for cases with sufficiently low Ra^* and high H_v values, as in the case of Fig. 16, a trend which is consistent with the lower relative height of the temperature peaks in the lower part of the channel that can be observed by comparing the upper and lower graphs of Fig. 18. Also note that, for a given $\bar{q}$ value, a reduction in the source length obviously produces more pronounced local extreme values in the wall temperature distribution, as can be observed by comparing Fig. 18(a) and (b). The same qualitative variation of the wall temperature distribution with Ra^*, H_v and s obtained in the case with $N = 5$ was also found in the case with $N = 2$ and different source lengths (the results are not presented here). From the above results, it can be concluded that, when a linear wall heat flux distribution is assumed, the heat sources with larger heat fluxes should be placed nearer the bottom of the channel in order to minimize the maximum wall temperature. Although a linear variation in the wall heat flux is the simplest way to introduce the effect of non-uniformity, and despite the optimization of a particular configuration would obviously depend on the possible restrictions in the number, strength and location of the

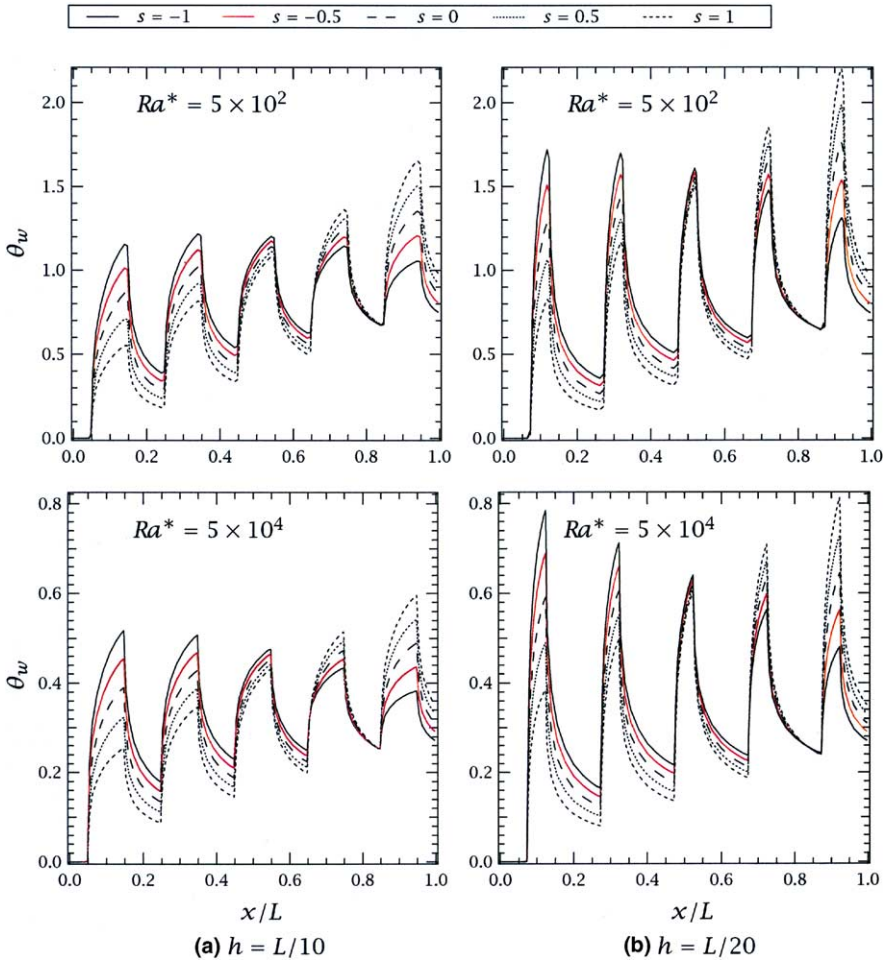

Fig. 18. Dimensionless temperature along the heated wall in the channel configuration of Fig. 17 with $N = 5$. The results correspond to two values of the source length, $h = L/10$ (a) and $h = L/20$ (b), and of the modified Rayleigh number, $Ra^* = 5 \times 10^2$ (upper graphs) and 5×10^4 (lower graphs), and different values of s ($b/L = 0.04$, $H_v = 1$).

heat sources, the analysis presented above provides significant insight into the influence of non-uniform wall heat flux distribution, especially when variable property effects are relevant.

5. Conclusions

The effects of variable properties (density, viscosity and conductivity) and non-uniform heating conditions on natural convective flows in vertical channels have been investigated. It was found that, for a given wall heat flux distribution law, the critical average wall heat flux for which the temperature in the channel increases sharply, varies appreciably with the modified Rayleigh number, reaching a maximum value for an intermediate Ra^* value between 10 and 100. The magnitude and location of this maximum depends on the wall heat flux distribution law. The numerical predictions of the maximum critical parameter $(H_v^2/Ra^*)_{\text{crit}}$ for linear heat flux distribution laws are in good agreement with the analytical estimations presented in this work. Distributions in which the wall heat flux decreases or increases with increasing height produce values of the critical average wall heat flux which are smaller and larger, respectively, than those corresponding to a uniform distribution. The greater the variation of the wall heat flux with height, the more the critical average wall heat flux departs from that corresponding to a uniform distribution. The critical values of the average wall heat flux obtained in this work represent lower limits, which would increase if three-dimensional, thermal radiation and streamwise heat conduction at the outlet and inlet channel sections were taken into account. The influence of variable property effects on the wall temperature distribution for non-uniform heating conditions has also been investigated. It

was found that, for a linear wall heat flux distribution and a given heating intensity, the maximum temperature at the wall can be minimized by making the wall heat flux slightly larger in the lower sections of the channel. Variable property effects may substantially increase wall temperature for certain heating conditions and affect the location of the maximum wall temperature.

References

[1] T. Aihara, S. Maruyana, J.S. Choi, Laminar free convection with variable fluid properties in vertical ducts of different cross-sectional shapes, in: C.L. Tien, V.P. Carey, J.K. Ferrel (Eds.), Heat Transfer, vol. 4, Hemisphere Publishing Corporation, 1986, pp. 1581–1586.

[2] A. Bar-Cohen, W.M. Rohsenow, Thermally optimum spacing of vertical, natural convection cooled, parallel plates, J. Heat Transfer 106 (1984) 116–123.

[3] N. Bianco, B. Morrone, S. Nardini, V. Naso, Air natural convection between inclined parallel plates with uniform heat flux at the walls, Heat Technol. 18 (2000) 23–45.

[4] D.R. Chenoweth, S. Paolucci, Natural convection in an enclosed vertical air layer with large horizontal temperature differences, J. Fluid Mech. 169 (1986) 173–210.

[5] A.M. Clausing, Natural convection correlations of heat transfer, J. Heat Transfer 107 (1985) 133–138.

[6] A.M. Clausing, S.N. Kempka, The influence of property variation on natural convection from vertical surfaces, J. Heat Transfer 103 (1981) 609–612.

[7] G. Desrayaud, A. Fichera, Laminar natural convection in a vertical isothermal channel with symmetric surface-mounted rectangular ribs, Int. J. Heat Fluid Flow 23 (2002) 519–529.

[8] A.F. Emery, J.W. Lee, The effects of property variations on natural convection in a square enclosure, J. Heat Transfer 121 (1999) 57–62.

[9] D.D. Gray, A. Giorgini, The validity of the Boussinesq approximation for liquids and gases, Int. J. Heat Mass Transfer 19 (1976) 545–551.

[10] Z.Y. Guo, Y.Z. Song, Z.X. Li, Laser speckle photography in heat transfer studies, Exp. Thermal Fluid Sci. 10 (1995) 1–16.

[11] Z.Y. Guo, Y.Z. Song, X.W. Zhao, Experimental investigation on natural convection in channel by laser speckle photography, Exp. Thermal Fluid Sci. 4 (1991) 594–600.

[12] Z.Y. Guo, X.B. Wu, Thermal drag and critical heat flux for natural convection of air in vertical parallel plates, J. Heat Transfer 115 (1993) 124–129.

[13] M.A. Leal, H.A. Machado, R.M. Cotta, Integral transform solutions of transient natural convection in enclosures with variable fluid properties, Int. J. Heat Mass Transfer 43 (2000) 3977–3990.

[14] K.T. Lee, Natural convection heat and mass transfer in partially heated vertical parallel plates, Int. J. Heat Mass Transfer 42 (1999) 4417–4425.

[15] B. van Leer, Towards the ultimate conservative difference scheme IV. A new approach to numerical convection, J. Comput. Phys. 23 (1977) 276–299.

[16] A. Pantokratoras, Laminar free-convection in water with variable physical properties adjacent to a vertical plate with uniform heat flux, Int. J. Heat Mass Transfer 46 (2003) 725–729.

[17] S.V. Patankar, D.B. Spalding, A calculation procedure for heat, mass, and momentum transfer in three-dimensional parabolic flows, Int. J. Heat Mass Transfer 15 (1972) 1787–1806.

[18] PHOENICS On-Line Information System. Available from: <http://www.cham.co.uk/phoenics/d_polis/d_lecs/general/intrlecs.htm>, Concentration Heat and Momentum Ltd., Wimbledon, London.

[19] E.M. Sparrow, J.L. Gregg, The variable fluid property problem in free convection, J. Heat Transfer 80 (1958) 879–886.

[20] S.A. Suslov, S. Paolucci, Stability of natural convection flow in a tall vertical enclosure under non-Boussinesq conditions, Int. J. Heat Mass Transfer 38 (1995) 2143–2157.

[21] H.Y. Wang, F. Penot, J.B. Sauliner, Numerical study of a buoyancy-induced flow along a vertical plate with discretely heated integrated circuit packages, Int. J. Heat Mass Transfer 40 (1997) 1509–1529.

[22] B. Zamora, J. Hernández, Influence of variable property effects on natural convection flows in asymmetrically-heated vertical channels, Int. Comm. Heat Mass Transfer 24 (1997) 1153–1162.

[23] B. Zamora, J. Hernández, Influence of upstream conduction on the thermally optimum spacing of isothermal, natural convection-cooled vertical plate arrays, Int. Comm. Heat Mass Transfer 28 (2001) 201–210.

[24] Z.Y. Zhong, K.T. Yang, J.R. Lloyd, Variable property effects in laminar natural convection in a square enclosure, J. Heat Transfer 107 (1985) 103–138.